Comparative study on the synergistic effect of POSS and graphene with melamine phosphate on the flame retardance of poly(butylene succinate)

Xin Wang[a,b], Yuan Hu[a,b,*], Lei Song[a], Hongyu Yang[a,b], Bin Yu [a],

Baljinder Kandola [c,*], Dario Deli [c]

[a] *State Key Laboratory of Fire Science, University of Science and Technology of China, Anhui 230026, P.R. China*
[b] *Suzhou Key Laboratory of Urban Public Safety, Suzhou Institute for Advanced Study, University of Science and Technology of China, Suzhou, Jiangsu 215123, P.R. China*
[c] *Institute for Materials Research and Innovation, University of Bolton, Deane Road, Bolton, BL3 5AB, United Kingdom*

Corresponding author at: State Key Laboratory of Fire Science, University of Science and Technology of China, 96 Jinzhai Road, Hefei, Anhui 230026, PR China.
Fax: +86 551 3601664.
E-mail address: yuanhu@ustc.edu.cn (Y. Hu) or B.Kandola@bolton.ac.uk (B. Kandola).

Abstract

Flame retardant poly(butylene succinate) (PBS) composites were prepared by melt blending PBS with melamine phosphate (MP), using graphene or polyhedral oligomeric silsesquioxanes (POSS) as synergists. The comparative study on the effect of POSS and graphene on the mechanical, thermal properties and flammability of flame retardant PBS was investigated. The addition of POSS or graphene further improved the LOI values of the flame retardant PBS, and V0 rating was obtained for the formulation containing 18 wt % MP and 2 wt% graphene. The incorporation of POSS and graphene reduced the crystallization of PBS, but improved the tensile strength. The presence of graphene exhibited superior thermal-oxidative resistance of the char layer compared to POSS, which effectively retarded the mass and heat transfer between the flame and the burning substrate, thus the heat release rate and total heat release of the flame retardant PBS composites containing graphene was significantly reduced during combustion.

Keywords: Poly(butylene succinate); POSS; Graphene; Thermal properties; Flame retardance

1. Introduction

The disposal problem of waste petroleum-derived plastics and increasing environmental concerns has motivated the development, production and application of biodegradable polymers [1]. Over the past few decades, considerable interest has been attracted on the poly(butylene succinate) (PBS) [2-5], one of the most promising and important biodegradable polymers produced from renewable resources at relatively

low cost and large production volume. Due to its superior mechanical and thermal properties, PBS has been widely used in biomedical materials, packaging, bags, films and fibers [6, 7]. However, like other aliphatic polyesters, PBS is highly combustible, which limits its application in automotive components, electronic or electrical industry. It is therefore necessary to provide fire resistance to PBS materials.

In recent years, incorporating nanoscale fillers into polymer composites has been extensively investigated to enhance not only their mechanical properties but also to improve thermal properties and to reduce flammability [8-10]. Among these nanoscale fillers, polyhedral oligomeric silsesquioxanes (POSS) has received great attention as one kind of effective flame retardant synergist with phosphorus-based compounds [11, 12]. The incorporation of POSS has obviously reduced the heat release rate, resulting from the formation of heat-resistant char layer. Very recently, some studies implied that graphene is another promising flame retardant nano-additive due to its unique two-dimensional (2D) atomic carbon sheet structure [13]. Because graphene has high aspect ratio in combination with its high intrinsic stiffness, it will reinforce polymers far more efficiently than conventional fillers. As is well known, the addition of nano-additives is to improve the flame retardant efficiency of polymer composites. It is reported that these two nano-additives, POSS and graphene, play a role of "barrier effect" in the condensed phase [11-13]. It is interesting to undertake a comparative study on the flame retardant efficiency between these two nano-additives.

The objective of this research is to compare the flame retardant effectiveness between POSS and graphene, using at a low concentrations (≤ 2wt%) in poly(butylene

succinate) containing melamine phosphate as a environmentally friendly flame retardant additive. The flammability and thermal properties of flame retardant PBS composites were evaluated by limiting oxygen index, UL-94, cone calorimetry and thermogravimetric analysis. Based on the observed performance of these two nano-additives in the composites, selective samples have been used to further study their flame retardant mechanism using thermogravimetric analysis-infrared spectrometry technique.

2. Experimental

2.1. Materials

Poly(butylene succinate) (PBS, weight-average molecular weight: 190000, hydroxyl end-capped) was purchased from Anqing Hexing Chemicals Co., Ltd. (Anhui, China). Melamine polyphosphate was provided by Shanghai Chemical Reagent Corp. (Shanghai, China). OctaAminophenyl polyhedral oligomeric silsesquioxanes (OpPOSS) was supplied by Shenyang Amwest Technology Company (Liaoning, China). Graphene powder was obtained from Hefei Keyan Chemicals Company (Anhui, China).

2.2. Preparation of samples

PBS, MP, POSS and graphene were dried in a vacuum oven at 80 °C overnight before compounding. The sample formulations are presented in Table 1. As an example, the fabrication of the sample PBS-6 is illustrated as follows: 40 g of PBS, 0.5 g of graphene and 9.5 g of MP were melt-blended in a twin-roller mill for 15 min; the temperature of the mill was maintained at 120 °C, and the roller speed was 30

rpm.The blended sample was hot-pressed at 120 °C under 10 MPa for 10 min into sheet with the thickness of 3.0 ± 0.1 mm. Other samples were fabricated using the same procedure. The formulations of all the samples are listed in Table 1.

2.3. Instruments and characterization

LOI was measured according to ASTM D2863. The apparatus used was an HC-2 oxygen index meter (Jiangning Analysis Instrument Co., China). The specimens used for the test were of dimensions $100 \times 6.5 \times 3$ mm^3. The vertical burning test was carried out on a CFZ-2 type instrument (Jiangning Analysis Instrument Co., China) according to the UL 94 test standard. The specimens used were of dimensions $130 \times 13 \times 3$ mm^3. Flammability of the samples was characterized by cone calorimeter (Fire Testing Technology, UK) according to ISO 5660. Samples were irradiated horizontally at a heat flux of 50 kW m^{-2}. All measurements were repeated three times and the results averaged.

Transmission electron microscopy analysis was conducted using a JEOL JEM-2100 instrument with an acceleration voltage of 100 kV. Scanning electron microscopy (SEM) was performed on the cross-sections of the samples using a Hitachi X650 scanning electron microscope. The specimens were previously coated with a conductive layer of gold. Tensile properties of the samples were tested with a WSM-20KB universal testing machine (Changchun, China) according to GB/T1040-92. At least five samples were tested to obtain average values. DSC analysis was carried out on a Q2000 analyzer (TA Co., USA). Each sample was heated from -40 °C to 200 °C at a heating rate of 10 °C/min. The nitrogen flow rate

was 50 ml/min. The crystallinity (χ_c) in all samples is calculated as follows:

$$\chi_c(\%) = \frac{\Delta H_m}{\Delta H_0} \times 100\%$$

where ΔH_m is the measured melting enthalpy (from DSC) and ΔH_0 is the enthalpy of pure PBS crystal (200 J/g) [14].

Thermogravimetric analysis (TGA) was performed on a SDT 2960 simultaneous DTA-TGA instrument from room temperature to 600 ℃ using about 10.0 mg of samples heated at constant heating rate of 10 °C/min. The samples were run in triplicate; the temperature reproducibility of the instrument is $\pm$ 1 °C while the mass reproducibility is $\pm 0.2\%$. The theoretical TG curve was computed by linear combination between the TG curves of neat PBS, MP and nanofillers. The formula is as follows:

$$W_{th}(T)_{Composite} = x \times W_{\exp}(T)_{PBS} + y \times W_{\exp}(T)_{MP} + z \times W_{\exp}(T)_{Nanofiller}, x + y + z = 1.$$

where $W_{\exp}(T)_{PBS}$: experimental TG curve of the pure PBS; $W_{\exp}(T)_{MP}$: experimental TG curve of MP; $W_{\exp}(T)_{nanofiller}$: experimental TG curve of graphene or POSS; x, y, and z are the weight percentages of the PBS, MP, and nanofiller in the composites, respectively.

TG-IR was performed using the SDT 2960 simultaneous thermogravimetric analyzer that was linked to the Nicolet Smart iTR iS10 FTIR spectrophotometer. About 10.0 mg of the sample was put in an alumina pans and heated from 30 to 600 °C. The heating rate was 10 °C/min (nitrogen atmosphere, flow rate of 100 ml/min).

3. Results and discussion

3.1. Morphology

Fig. 1 shows the TEM image of the sample PBS-1, PBS-4 and PBS-7. In Fig. 1(a) melamine phosphate particles of about 0.2 μm size can be clearly seen. Fig. 1(b) clearly shows many POSS particles (indicated by the white circles) with a wide size distribution in the range of 10-100 nm, suggesting that the POSS does not disperse at a molecular level in the matrix but still at a nanoscale level. As can be observed from Fig. 1(c), graphene sheets are uniformly dispersed with a average size of 0.25 um in the PBS.

3.2. Mechanical properties

The data for the tensile strength and elongation at break of the PBS and flame retardant PBS composites were obtained from the computer controlled universal tensile testing machine. The data for the mechanical properties are summarized in Table 2. It can be seen that the tensile strength is reduced after the addition of 20.0 wt% MP. As is well known, the additives at high loading usually cause a negative impact on the mechanical properties of the polymer matrix, which is also reported in earlier literature [15, 16]. However, the incorporation of nano-additives exhibits reinforcement on the PBS, which could be attributed to the strong interfacial interaction between the nanofillers and PBS matrix. Moreover, the flame retardant PBS composites with nano-additives exhibit smaller elongation at break compared to the virgin ones.

To evaluate the effect of POSS and graphene on the mechanical properties of the PBS matrix, SEM is employed to investigate the fracture surfaces of the samples. Fig.

2 shows SEM images of the fractured surface of PBS, PBS-1, PBS-4 and PBS-7. As can be observed from Fig. 2(a), pure PBS displays a very smooth surface due to the brittleness of semicrystalline PBS. Fig. 2(b) shows a rough fracture surface of PBS-1, but there is no clear agglomeration of melamine phosphate. After adding POSS and graphene, much rougher fracture surface is observed from Fig. 2(c) and (d), indicating that the nano-additives have stronger interfacial interactions with PBS matrix.

3.3. Effect of nano-additives on the crystallinity of PBS

Since PBS is a semicrystalline polymer [17], its mechanical properties should strongly depend on its crystallinity. Therefore, DSC is employed to investigate the influence of incorporating fillers on the crystallinity behaviors of pure PBS and its composites. Fig. 3 gives DSC thermograms during the second heating cycle, and the relevant data are summarized in Table 3. The melting temperature (T_m) of pure PBS is 109.7 $^{\circ}$C, and no significant change of T_m for flame retardant PBS is observed, indicating that the incorporation of flame retardant additives exhibits little influence on the T_m of PBS. The crystallinity of flame retardant PBS composites is reduced after adding the nanofillers. Generally, the reduction of crystallinity has a negative impact on the mechanical properties of the composites. However, the increased tensile strength of PBS composites is observed after adding the nanofillers, which can be probably attributed to the nano-reinforced effect of graphene and POSS in the polymer matrix and strong interfacial interactions between both components [18].

3.4. Thermal-oxidative properties of flame retardant PBS samples

The typical TG and DTG traces for pure PBS and flame retardant PBS

composites with POSS and graphene under air atmosphere are presented in Fig. 4 and Fig. 5, respectively. The onset decomposition temperature (T_d) can be defined as the temperature at which the weight loss is 5%. The relative thermal stability of the samples was evaluated by the temperature of 5% weight loss, the temperature of maximum rate of weight loss (T_{max}) and the percent char yield at 550 ^{o}C. These data are listed in Table 4.

The onset decomposition temperature for virgin PBS is 354 ^{o}C, and its TGA trace shows only one weight-loss stage. The stage is in the temperature range of 330-430 ^{o}C corresponding to a single DTG peak at 410 ^{o}C (T_{max}) and the weight loss is about 99.6 % leaving no char residue. For the flame retardant PBS sample containing MP only, the T_d is lower than PBS, due to the early decomposition of melamine phosphate (T_d = 264 ^{o}C) [19], which then interacts with PBS and helps in improving the char yield.

In the case of the flame retardant PBS composites with POSS and graphene, their thermal degradation process presents two mass loss steps in the temperature range of 300-350 ^{o}C and 350-400 ^{o}C. The first mass loss step is ascribed to the decomposition of MP (~15wt% loss) while the second is attributed to the decomposition of PBS matrix. The T_d of PBS composites is around 330 ^{o}C, which is lower than that of PBS, indicating the presence of MP could catalyze the decomposition of PBS before 350 ^{o}C. Furthermore, the T_{max} of PBS composites is also lower than pure PBS. However, the residual char is increased in all samples compared to PBS-1 (melamine phosphate containing sample). The best result is shown by flame retardant PBS sample

containing 2wt% graphene with 14% char yield. The well dispersed and special structure of graphene in the polymer matrix is expected to be an effective barrier to the permeation of flammable gases. Similar result was also found in previous graphene-based nanocomposites [20, 21]. Hence, it can be deduced that the incorporation of graphene into the PBS matrix is beneficial to promote the formation of char layer and improve the thermal-oxidative stability of the char.

To further investigate the MP-nanofiller synergism, the weight difference between the experimental and theoretical TG curves for PBS-4 and PBS-7 are presented in Fig. 6. As can be seen, T_d in the experimental curves is higher than that in the calculated ones, suggesting the improvement of thermal-oxidative stability. However, at the temperature range of 380~500 ℃, the experimental curves show faster thermal degradation process than the calculated ones. Because the calculated curves are obtained by linear combination among the noninteracting individual components in the system [22], actually, the catalyzing effect of MP on the depolymerization of PBS indeed occurs.

3.5. Flammablity

The effect of POSS and graphene on the LOI values and UL-94 results of the flame retardant PBS composites is presented in Table 1. Pure PBS exhibits an LOI value of 23.0% and is highly combustible, showing no classification in the UL-94 test. When 20 wt% of MP is added, the LOI value of PBS-1 goes up to 31.5%, but it still does not pass the UL-94 V0 rating. Adding POSS shows a slight increase in LOI value compared to that of PBS-1. When 0.5-2.0 wt% of MP is substituted by graphene,

LOI value is higher than that with melamine phosphate alone. An optimum is observed at 2.0 wt% of graphene and 18.0 wt% of MP, which can pass the UL-94 V0 rating in vertical burning test. In the presence of melamine phosphate, each nano-additive produces a higher relative increases in LOI values. At the high loadings of the nano-additive (≥ 1.0 wt%), the flame retardant effect of graphene is superior to that of POSS.

Cone calorimeter tests provide abundant information on the combustion properties of the investigated materials, including the time-to-ignition (TTI); the heat release rate, and in particular the peak value (PHRR); the time-to-PHRR (tPHRR); the total heat release (THR); the mass loss; and the amount of smoke produced during combustion. These data and some derived parameters such as the Fire Growth Rate Index (FIGRA) are presented in Table 5. Fig. 7 illustrates the HRR, the THR and the mass loss as functions of time for formulations filled with POSS (a, b and c) and graphene (d, e and f).

After ignition, PBS shows one single well-defined peak in the HRR curve with the peak value of 1144 kW/m^2. Presence of MP in PBS-1 decreases the PHRR value of PBS by 40% and increases the time-to-PHRR. Prior to the PHRR, there is a shoulder peak in HRR curves. In the formulation containing 0.5wt% POSS (PBS-2), there is no significant change in PHRR compared to PBS-1 and also adding more POSS results n no further decrease in PHRR. Combining graphene and MP in PBS results in a significant decrease in PHRR and THR values. For the sample PBS-7, the PHRR and THR are significantly reduced, by 63% and 23%, respectively, compared

to those of pure PBS.

Fig. 8 presents the digital photos of the residue char for all samples after the cone calorimeter tests. Apparently, pure PBS leaves no residue char after burning and flame retarded PBS with MP alone gives the cracked char residue. With the addition of POSS, flame retardant PBS composites produce more char residue relative to the former systems, but the central part of this char layer still burns, indicating the poor thermal-oxidative resistance. While for flame retardant PBS containing 2wt% graphene, a continual and swelling char forms, which can prevent the heat and mass transfer between the flame and the polymer substrate, and thus protect the underlying materials from further burning and retard the pyrolysis of polymers. As a result, PHRR and THR values are significantly reduced.

As can be observed from Fig. 7 and Table 5, the TTI of the flame retardant PBS decreases compared to pure PBS, while the tPHRR increases. The decrease of the TTI for the flame retardant PBS in comparison with the PBS matrix is probably due to the presence of MP and nanoparticles might catalyse the PBS decomposition. The increase of the tPHRR can be attributed to the formation of a more stable char barrier, which efficiently retards the heat and mass transfer in fire. Moreover, the combustion time increases from 115 s for pure PBS to 134 s and 149 s for the PBS-4 and PBS-7, respectively, implying the improved flame resistance.

The fire growth rate index (FIGRA), which indicates the burning propensity of a material, has been calculated from the ratio of PHRR and time to PHRR for all samples in Table 5. It can be clearly seen that graphene is more effective in reducing

the fire growth compared to POSS. The FIGRA value further decreases with higher loading of graphene. With regard to smoke production, all the samples containing flame retardant show higher total smoke production compared to pure PBS. The increase in smoke formation in flame retarded samples is due to incomplete combustion of the resin formulation.

The overall fire performance from cone calorimetry of different samples is evaluated by plotting the THR versus the ratio of PHRR to TTI as shown in Fig. 9. The THR represents the propensity for fire to burn over a prolonged time period while PHRR/TTI represents the rate of fire growth [23]. With the direction that the arrow points to, the flame retarded samples have better fire performance. It can be seen that PBS-7 has best flame resistance.

Based on the results discussed, it could be concluded that graphene shows more effective fire retardance than POSS in combination with MP. Combining MP and graphene significantly decreases the PHRR, the THR, the mass loss rate and FIGRA, which is attributed to the barrier effect of graphene on the formation of char residue.

3.6. Volatilized products of PBS and flame retardant PBS analyzed by TG-FTIR

The TG-FTIR technique can give information about the pyrolysis products, which provides insight into the thermal degradation mechanisms. In this study, the PBS, PBS-4 and PBS-7 samples are chosen to perform TG-FTIR tests to identify its gas products during the thermal degradation, with pure PBS as the control sample.

The FTIR spectra obtained at the maximum evolution rate for the PBS, PBS-4 and PBS-7 are shown in Fig. 10. Some of the gaseous decomposition products of the

PBS are unambiguously identified by characteristic strong FTIR signals, such as -CH$_2$- groups of succinic acid and butanediol (2820-2980 cm^{-1}), CO$_2$ (2360 cm^{-1}), succinic anhydride (1810 and 1760 cm^{-1}), and aliphatic ethers (1100-1250 cm^{-1}) [24, 25]. Moreover, it can be seen that the peak at around 1810 cm^{-1} splits into two bands. This is mainly caused by different products containing carbonyl group being formed during the degradation of PBS, including carboxylic acid and anhydride (1750 and 1820 cm^{-1}) [25]. It is well-known that depolymerization is the main process associated with the thermal degradation of polyesters. In the process of depolymerization, the main decomposition products of PBS are succinic acid and butanediol, CO$_2$, succinic anhydride, and aliphatic ethers.

The FTIR spectra of pyrolysis products of PBS-4 and PBS-7 at the maximum evolution rate exhibit characteristic bands of CO$_2$ (2360 cm^{-1}), succinic acid and butanediol (-OH groups: 3400-3700 cm^{-1} and -CH$_2$- groups: 2980-2850 and 1200-1300 cm^{-1}), succinic anhydride (1750 and 1820 cm^{-1}), which is similar to those of pure PBS. Additionally, the appearance of the new absorption band at 927 cm^{-1} is attributed to the the release of NH$_3$ derived from MP, which is overlapped by the bands of C-H deformation vibration of gaseous alkene [25]. Ammonia is effective for depolymerization of polyesters, such as poly(ethylene terephthalate) and polylactide [26, 27]. As is also well-known, polyesters are sensitive to acidic species, which catalyses the depolymerization of macromolecular chain, especially at higher temperature, as shown schematically below:
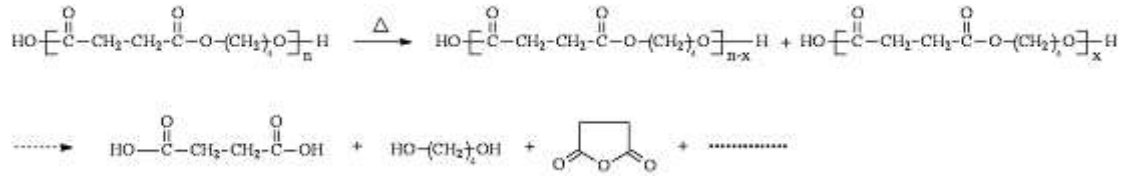
The absorbance of pyrolysis products for PBS, PBS-4 and PBS-7 vs time is revealed in Fig. 11. It can be seen that the maximum evolution rate of pyrolysis products for PBS-4 and PBS-7 occurs at 36.0 min and 34.0 min, respectively, which is earlier than that of pure PBS (39.0 min). This can be interpreted that the presence of MP catalyzes the thermal decomposition of PBS. The acidic species and ammonia degraded from MP promote the formation of a protective char layer, which could prevent the combustible gases from transferring to the surface of the materials and feed the flame. Meanwhile, the release of nonflammable gases (such as CO_2 and NH_3) can dilute the combustible gas, thus reduce the HRR and THR values.

4. Conclusion

POSS and graphene were used as nanofillers to produce flame retardant poly(butylene succinate) composites by melt blending. The addition of graphene exhibited superior flame retardance to POSS. With 18wt% MP and 2w% graphene, PBS can achieve the LOI value of 34.0% and UL-94 V0 grade. Though the presence of nanofillers reduced the crystallization of PBS, the tensile strength of flame retardant PBS composites showed insignificant reduction compared with that of pure PBS due to the strong interfacial interactions between nanofillers and PBS matrix. The results from TGA and cone calorimeter indicated that the addition of both POSS and graphene improved the char yield, but incorporating graphene into PBS displayed better thermal-oxidative resistance in char layer. TG-FTIR results showed that the

15

main decomposition products of PBS-7 were hydrocarbons, CO_2, acid anhydride and aliphatic ethers, which was similar to those of PBS, however, much less flammable gas products were released relative to pure PBS. Compared with POSS, graphene exhibited better combined properties of mechanical, thermal and flame retardant behaviors due to the nano-reinforcement and barrier effect of its unique structure, which was more suitable to manufacture flame retardant PBS composites.

Acknowledgments

References

[1] E. Gallo, B. Schartel, D. Acierno, P. Russo, Flame retardant biocomposites: Synergism between phosphinate and nanometric metal oxides, Eur. Polym. J. 47 (2011) 1390-1401.

[2] Y. Tachibana, T. Masuda, M. Funabashi, M. Kunioka, Chemical synthesis of fully biomass-based poly(butylene succinate) from inedible-biomass-based furfural and evaluation of its biomass carbon ratio, Biomacromolecules 11 (2010) 2760-2765.

[3] S.S. Ray, K. Okamoto, M. Okamoto, Structure-property relationship in biodegradable poly(butylene succinate)/layered silicate nanocomposites, Macromolecules 36 (2003) 2355-2367.

[4] G.Z. Papageorgiou, D.N. Bikiaris, Crystallization and melting behavior of three biodegradable poly(alkylene succinates): A comparative study, Polymer 46 (2005) 12081-12092.

[5] T. Bin, J.P. Qu, L.M. Liu, Y.H. Feng, S.X. Hu, X.C. Yin, Non-isothermal crystallization kinetics and dynamic mechanical thermal properties of poly(butylene succinate) composites reinforced with cotton stalk bast fibers, Thermochim. Acta 525 (2011) 141-149.

[6] A.A. Shah, F. Hasan, A. Hameed, S. Ahmed, Biological degradation of plastics: A comprehensive review, Biotechnol. Adv. 26 (2008) 246-265.

[7] A.K. Mohanty, M. Misra, G. Hinrichsen, Biofibres, biodegradable polymers and biocomposites: An overview, Macromol. Mater. Eng. 276 (2000) 1-24.

[8] Y.C. Chiu, F.Y. Liu, C.C. M. Ma, I.C. Chou, L. Riang, C.L. Chiang, J.C. Yang, Syntheses and characterization of novel P/Si polysilsesquioxanes/epoxy nanocomposites, Thermochim. Acta 473 (2008) 7-13.

[9] M. Pluta, J.K. Jeszka, G. Boiteux, Polylactide/montmorillonite nanocomposites: Structure, dielectric, viscoelastic and thermal properties, Eur. Polym. J. 43 (2007) 2819-2835.

[10] J.W. Gilman, W.H. Awad, R.D. Davis, J. Shields, R.H. Harris, C. Davis, A.B. Morgan, T.E. Sutto, J. Callahan, P.C. Trulove, H.C. DeLong, Polymer/layered silicate nanocomposites from thermally stable trialkylimidazolium-treated montmorillonite, Chem. Mater. 14 (2002) 3776-3785.

[11] A. Vannier, S. Duquesne, S. Bourbigot, A. Castrovinci, G. Camino, R. Delobel, The use of POSS as synergist in intumescent recycled poly(ethylene terephthalate), Polym. Degrad. Stabil. 93 (2008) 818-826.

[12] X. Wang, Y. Hu, L. Song, W.Y. Xing, H.D. Lu, Thermal degradation behaviors of epoxy resin/POSS hybrids and phosphorus-silicon synergism of flame retardancy, J. Polym. Sci. Pol. Phys. 48 (2010) 693-705.

[13] G.B. Huang, J.R. Gao, X. Wang, H.D. Liang, C.H. Ge, How can graphene reduce the flammability of polymer nanocomposites? Mater. Lett. 66 (2012) 187-189.

[14] T. Miyata, T. Masuko, Crystallization behaviour of poly(tetramethylene succinate), Polymer 39 (1998) 1399-1404.

[15] H. Shen, Y.H. Wang, K.C. Mai, Effect of compatibilizers on thermal stability and mechanical properties of magnesium hydroxide filled polypropylene composites, Thermochim. Acta 483 (2009) 36-40.

[16] N.A. Isitman, C. Kaynak, Nanoclay and carbon nanotubes as potential synergists of an organophosphorus flame-retardant in poly(methyl methacrylate), Polym. Degrad. Stabil. 95 (2010) 1523-1532.

[17] T. Dong, Y. He, B. Zhu, K.M. Shin, Y. Inoue, Nucleation mechanism of alpha-cyclodextrin-enhanced crystallization of some semicrystalline aliphatic polymers, Macromolecules 38 (2005) 7736-7744.

[18] Y.X. Xu, W.J. Hong, H. Bai, C. Li, G.Q. Shi, Strong and ductile poly(vinyl alcohol)/graphene oxide composite films with a layered structure, Carbon 47 (2009) 3538-3543.

[19] W.Y. Chen, Y.Z. Wang, F.C. Chang, Thermal and flame retardation properties of melamine phosphate-modified epoxy resins, J. Polym. Res. 11 (2004) 109-117.

[20] J.J. Liang, Y. Huang, L. Zhang, Y. Wang, Y.F. Ma, T.Y. Guo, Y.S. Chen, Molecular-level dispersion of graphene into poly(vinyl alcohol) and effective reinforcement of their nanocomposites, Adv. Funct. Mater. 19 (2009) 2297-2302.

[21] H. Kim, Y. Miura, C.W. Macosko, Graphene/polyurethane nanocomposites for improved gas barrier and electrical conductivity, Chem. Mater. 22 (2010) 3441-3450.

[22] M. Bras, S. Bourbigot, C. Delporte, New intumescent formulations of fire-retardant polypropylene-discussion of the free radical mechanism of the

formation of carbonaceous protective material during the thermo-oxidative treatment of the additives, Fire Mater. 20 (1996) 191-203.

[23] R.V. Petrella, The assessment of full-scale fire hazards from cone calorimeter data, J. Fire Sci. 12 (1994) 14-43.

[24] K. Wu, Y. Hu, L. Song, H.D. Lu, Z.Z. Wang, Flame retardancy and thermal degradation of intumescent flame retardant starch-based biodegradable composites, Ind. Eng. Chem. Res. 48 (2009) 3150-3157.

[25] Y.J. Chen, J. Zhan, P. Zhang, S.B. Nie, H.D. Lu, L. Song, Y. Hu, Preparation of intumescent flame retardant poly(butylene succinate) using fumed silica as synergistic agent, Ind. Eng. Chem. Res. 49 (2010) 8200-8208.

[26] K. Zenda, T. Funazukuri, Depolymerization of poly(ethylene terephthalate) in dilute aqueous ammonia solution under hydrothermal conditions, J. Chem. Technol. Biotechnol. 83 (2008) 1381-1386.

[27] F. Wang, H. Tsuno, T. Hidaka, J. Tsubota, Promotion of polylactide degradation by ammonia under hyperthermophilic anaerobic conditions, Bioresource Technol. 102 (2011) 9933-9941.

Captions

Table 1. Formulations and flame retardancy of PBS and flame retardant PBS.

Table 2. Mechanical properties of PBS and flame retardant PBS composites.

Table 3. DSC data of PBS and flame retardant PBS composites.

Table 4. TG data of PBS and flame retardant PBS composites in air atmosphere.

Table 5. Cone calorimeter results for flame retardant PBS composites at 50 kWm^{-2} heat flux.

Figure 1. TEM images of (a) PBS-1; (b) PBS-4; (c) PBS-7.

Figure 2. SEM images of the fractured surface of (a) PBS, (b) PBS-1, (c) PBS-4 and (d) PBS-7: (1) × 500 and (2) × 2000.

Figure 3. Melting peaks of pure PBS and flame retardant PBS composites obtained from DSC curves.

Figure 4. TG and DTG profiles of PBS and flame retardant PBS containing POSS composites under air atmosphere.

Figure 5. TG and DTG profiles of PBS and flame retardant PBS containing graphene composites under air atmosphere.

Figure 6. Weight difference between the experimental and theoretical TG curves for (a) PBS-4 and (b) PBS-7.

Figure 7. Heat release rate, total heat release, and mass loss versus time curves for PBS and flame retardant PBS/POSS (a, b, c) and flame retardant PBS/graphene (d, e, f).

Figure 8. Digital photos of cone burnt samples of PBS and flame retardant PBS composites after 300 sec of cone calorimeter test.

Figure 9. Fire performance evaluation of different samples in accordance to a plot of total heat release (fire duration) and PHRR/TTI (propensity to cause a rapidly
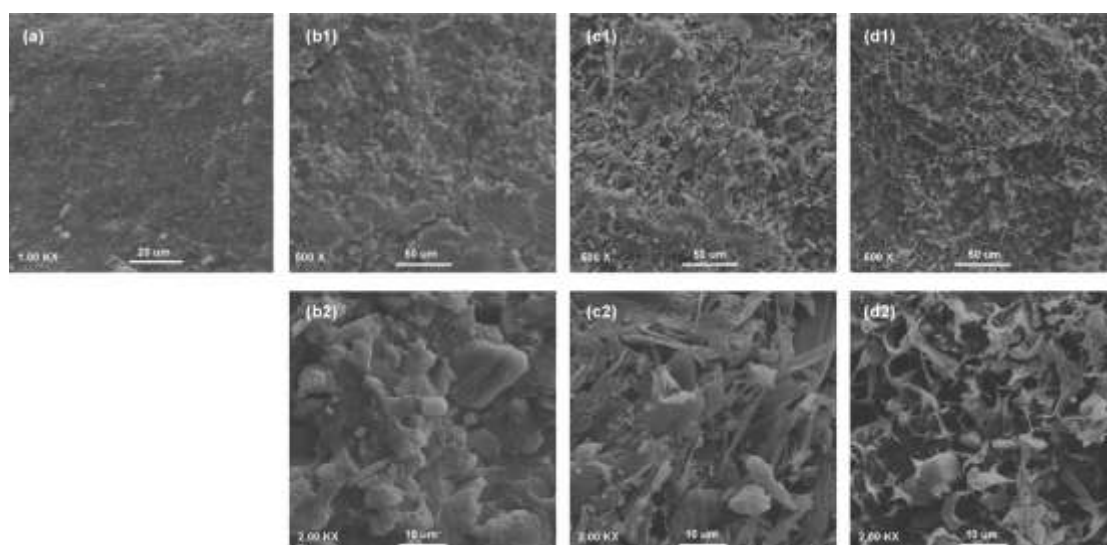
growing fire) on exposure to a 50 kW/m^2 heat flux.

Figure 10. FTIR spectra of PBS, PBS-4 and PBS-7 at the maximum evolution rate.

Figure 11. Absorbance of pyrolysis products for PBS, PBS-4 and PBS-7 vs time: hydrocarbons; CO$_2$; carbonyl compounds and ethers.
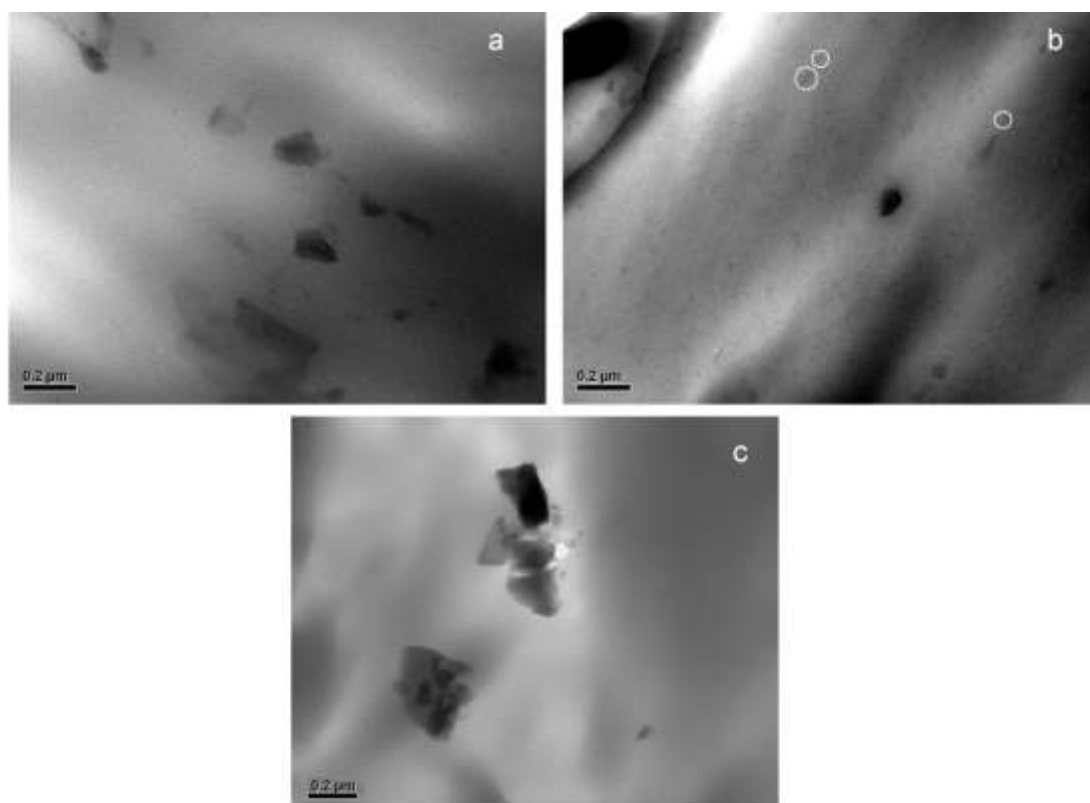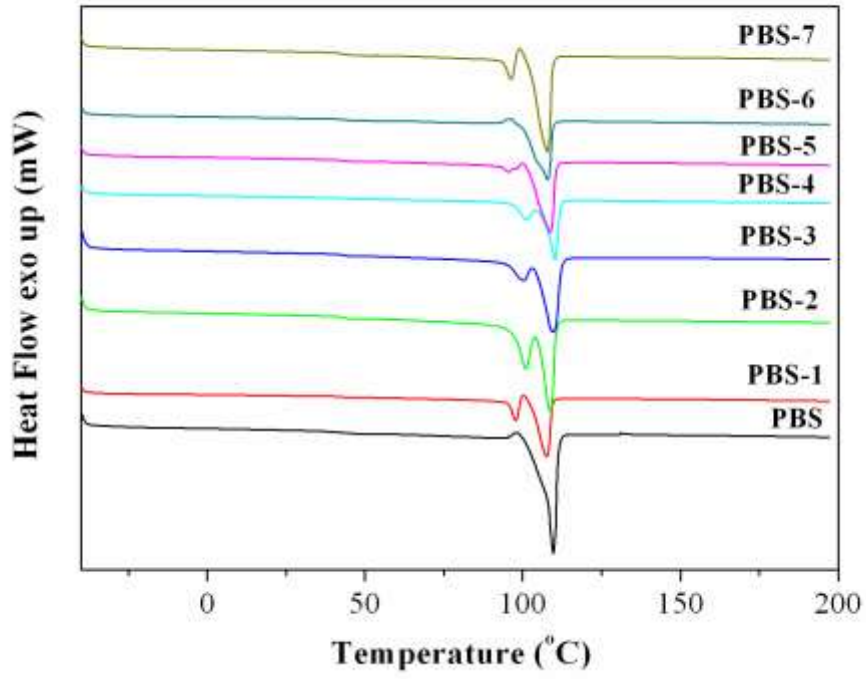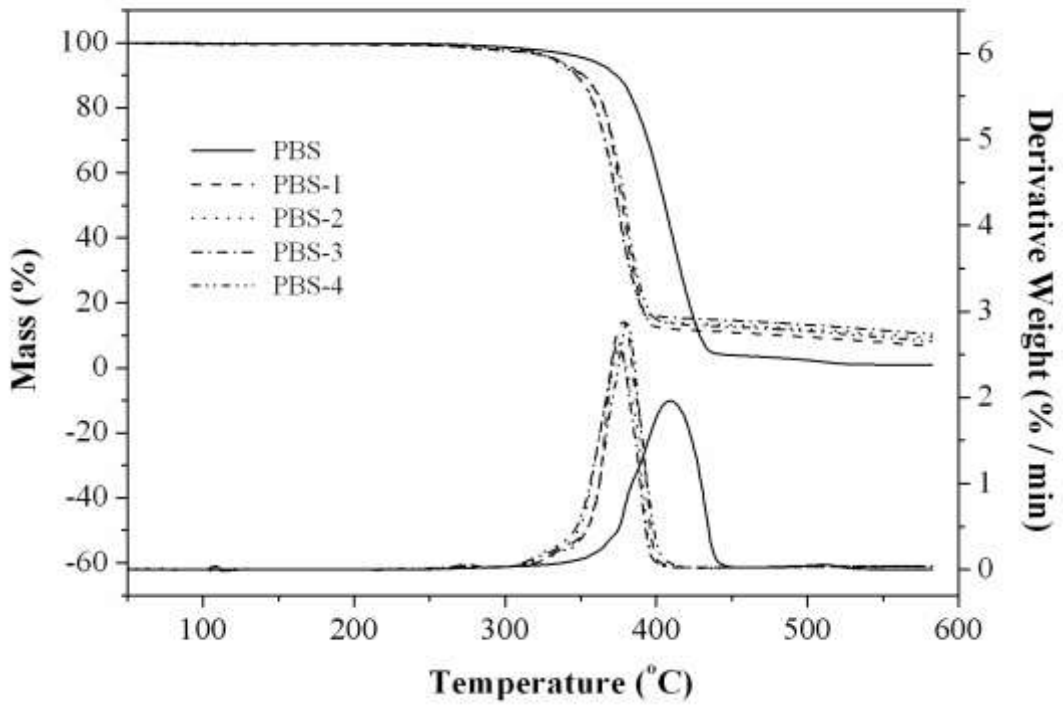

Figure 1

Figure 2

22

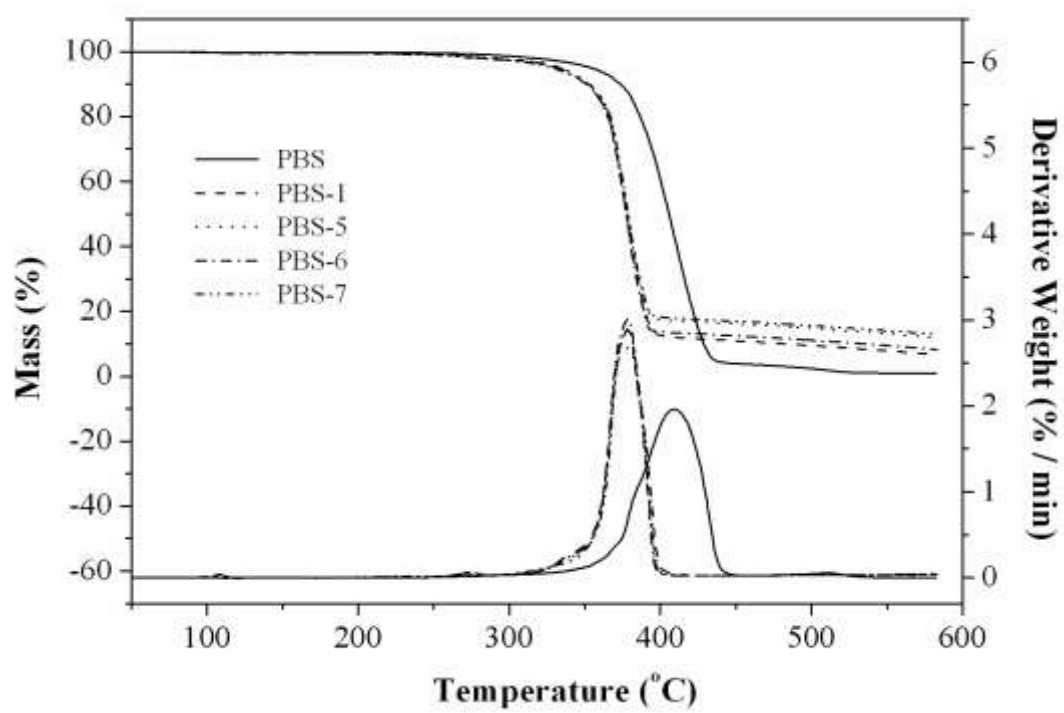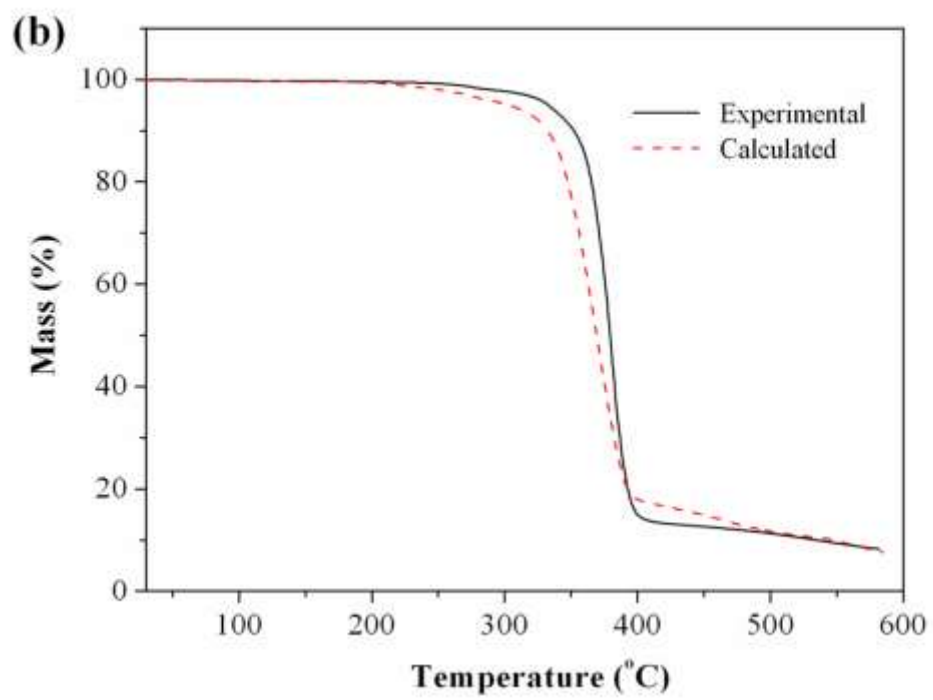**Figure 3**

Figure 4

Figure 5
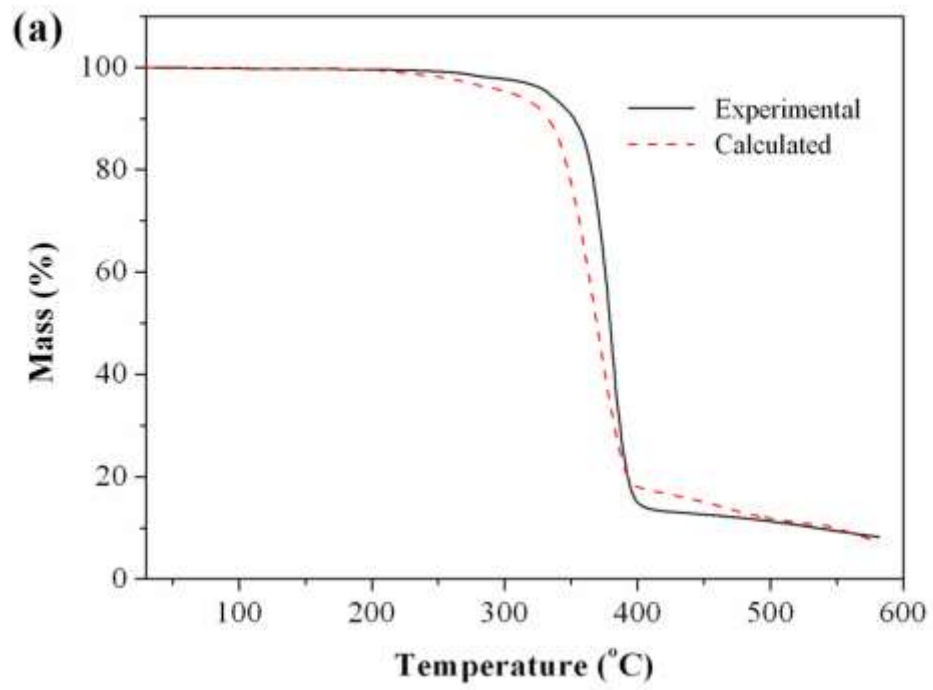
Figure 6
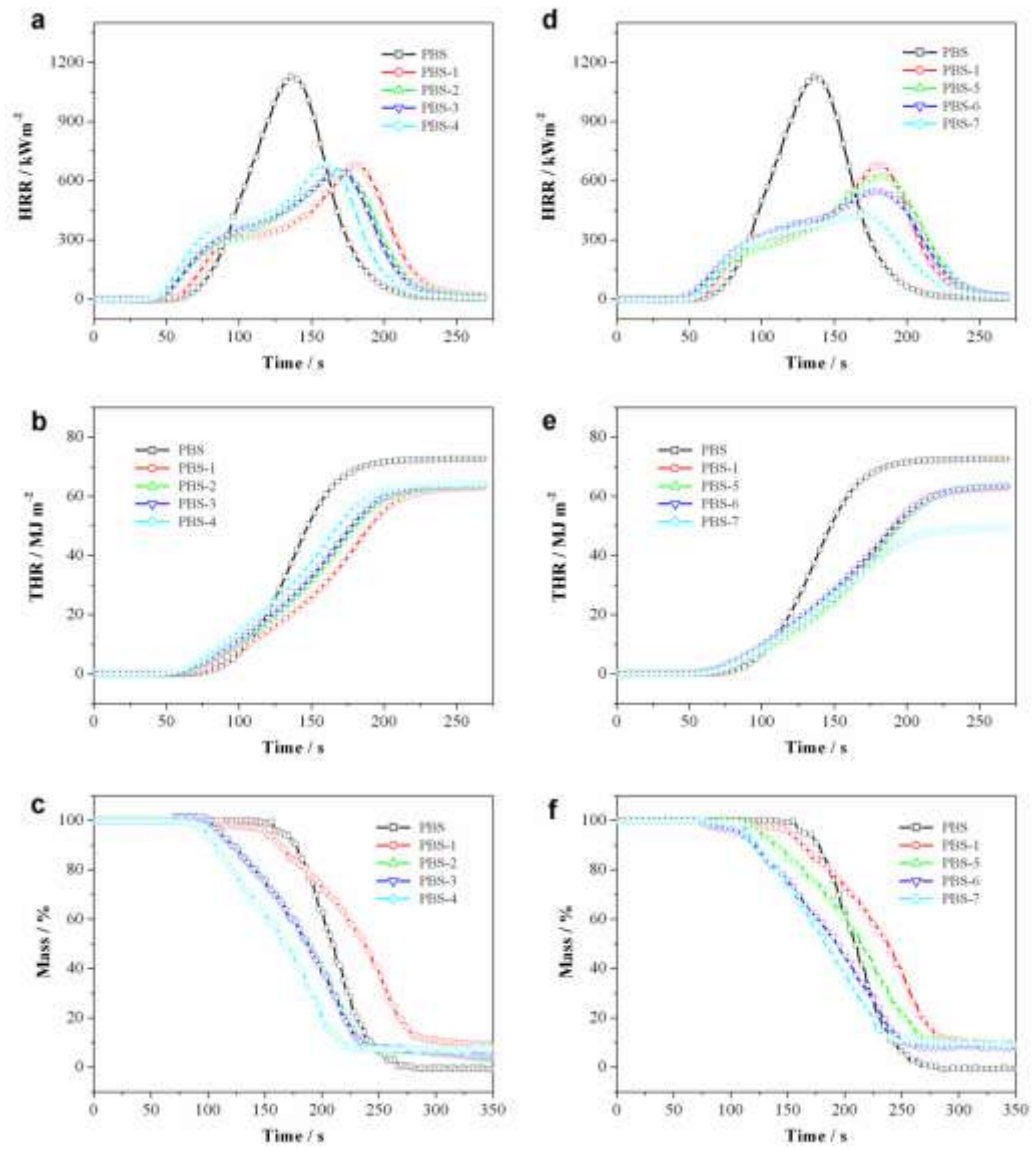
Figure 7
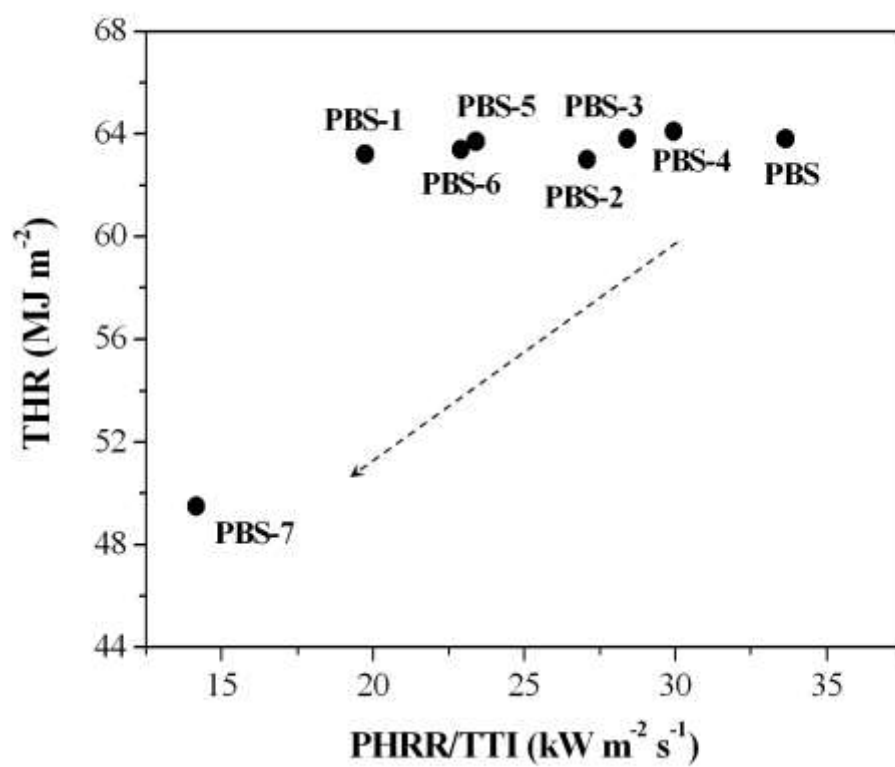
Figure 8

Figure 9
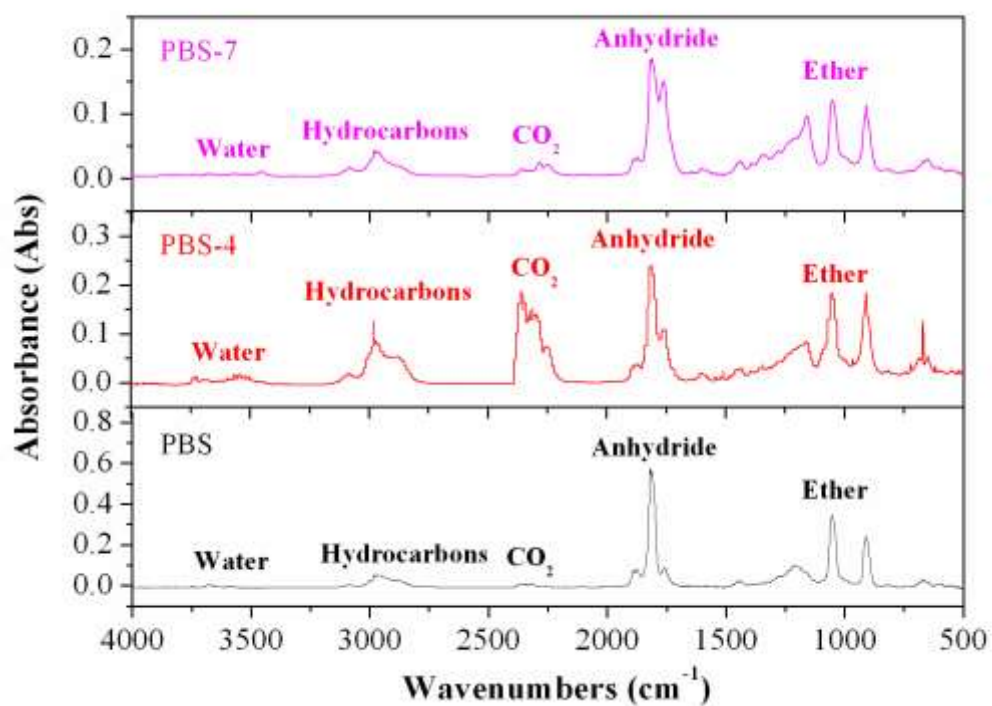
Figure 10
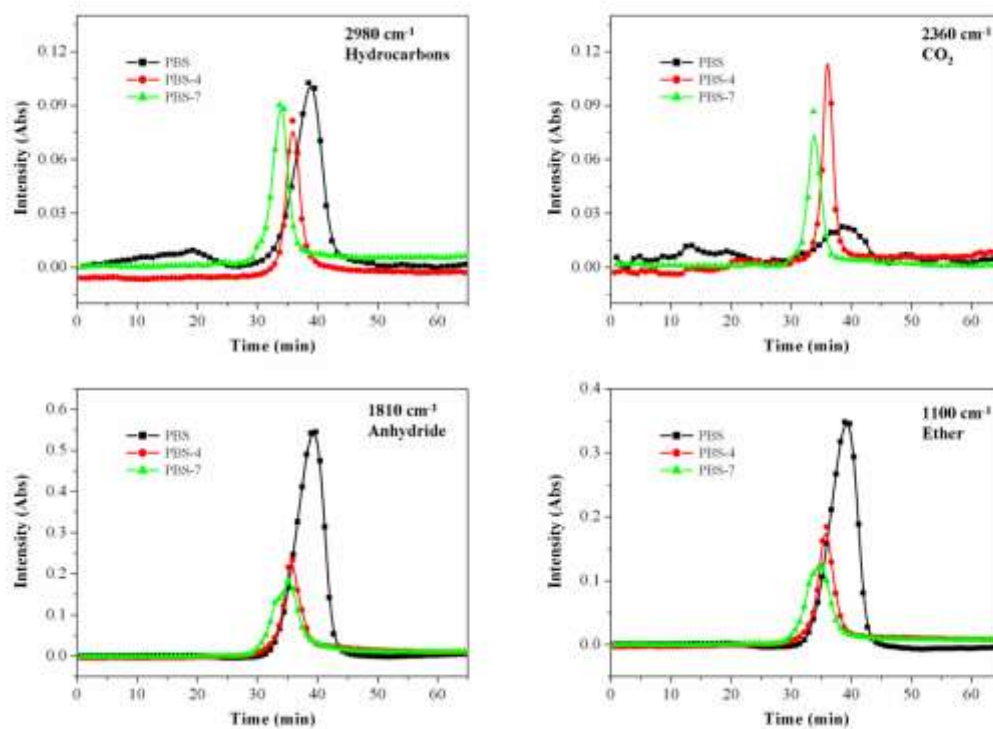
Figure 11

Table 1. Formulations and flame retardancy of PBS and flame retardant PBS.

Samples	Composition (wt%)				Flame retardancy		
	PBS	MP	POSS	Graphene	LOI ± 0.5 (%)	ΔLOI [a] (%)	UL-94 rating
PBS	100	0	0	0	23.0	--	NR
PBS-1	80	20	0	0	31.5	8.5	V1
PBS-2	80	19.5	0.5	0	32.5	9.5	V1
PBS-3	80	19	1.0	0	32.0	9.0	V1
PBS-4	80	18	2.0	0	33.0	10.0	V1
PBS-5	80	19.5	0	0.5	32.0	9.0	V1
PBS-6	80	19	0	1.0	33.5	10.5	V1
PBS-7	80	18	0	2.0	34.0	11.0	V0

[a]ΔLOI = LOI of sample - LOI of PBS.

Table 2. Mechanical properties of PBS and flame retardant PBS composites.

Samples	Tensile strength (MPa)	Elongation at break (%)
PBS	30.8 ± 0.4	17.9 ± 1.2
PBS-1	23.7 ± 0.3	10.5 ± 0.6
PBS-2	24.5 ± 0.5	12.2 ± 1.1
PBS-3	26.3 ± 0.3	10.6 ± 0.8
PBS-4	29.6 ± 0.6	8.3 ± 0.7
PBS-5	25.4 ± 0.8	11.4 ± 1.3
PBS-6	28.9 ± 0.3	12.2 ± 1.5
PBS-7	30.2 ± 0.6	9.5 ± 0.4

Table 3. DSC data of PBS and flame retardant PBS composites.

Samples	T_m (^{o}C)	ΔH_m (J/g)	Xc (%)
PBS	109.7	55.1	27.5
PBS-1	107.6	38.1	19.1
PBS-2	108.9	37.7	18.9
PBS-3	109.8	33.1	16.6
PBS-4	110.3	26.6	13.3
PBS-5	108.8	51.6	25.8
PBS-6	107.9	50.2	25.1
PBS-7	107.8	43.4	21.7

Table 4. TG data of PBS and flame retardant PBS composites in air atmosphere.

Samples	$T_d \pm 0.5$ (^{o}C)	$T_{max} \pm 1.0$ (^{o}C)	Char residue at 550 ^{o}C $\pm$ 0.5 (%)
PBS	354	410	0.4
PBS-1	333	378	7.8
PBS-2	331	376	10.4
PBS-3	332	374	11.5
PBS-4	332	380	9.4
PBS-5	334	378	13.1
PBS-6	331	379	11.5
PBS-7	329	379	14.0

Table 5. Cone calorimeter results for flame retardant PBS composites at 50 kWm^{-2} heat flux.

Samples	TTI (s) ± 2	Flameout (s) ± 2	Peak HRR (kW m^{-2}) ± 30	FIGRA (kW m^{-2} s^{-1})	THR (MJ m^{-2}) ± 0.5	Smoke (m^2 m^{-2}) ± 10	
						at 60s	at 180s
PBS	34	149	1144	8.2	63.8	34	470
PBS-1	35	192	691	3.8	63.2	92	619
PBS-2	24	171	650	3.9	63.0	106	596
PBS-3	24	162	682	4.0	63.8	102	687
PBS-4	23	157	689	4.4	62.1	142	743
PBS-5	27	198	632	3.5	63.7	46	490
PBS-6	24	191	550	3.1	63.4	73	596
PBS-7	30	181	425	2.6	49.5	98	578